Nuclear Engineering and Technology 55 (2023) 1885–1891

Contents lists available at ScienceDirect

Nuclear Engineering and Technology

journal homepage: www.elsevier.com/locate/net

Original Article

Impacts of the calcination temperature on the structural and radiation shielding properties of the NASICON compound synthesized from zircon minerals

Islam G. Alhindawy [a, **], Hany Gamal [a], Aljawhara.H. Almuqrin [c], M.I. Sayyed [d, e], K.A. Mahmoud [a, b, *]

[a] Nuclear Materials Authority, P.O. Box 530, El-Maadi, Cairo, Egypt
[b] Ural Federal University, 19 Mira St, 620002, Yekaterinburg, Russia
[c] Department of Physics, College of Science, Princess Nourah Bint Abdulrahman University, P.O.Box 84428, Riyadh, 11671, Saudi Arabia
[d] Department of Physics, Faculty of Science, Isra University, Amman, Jordan
[e] Department of Nuclear Medicine Research, Institute for Research and Medical Consultations (IRMC), Imam Abdulrahman Bin Faisal University (IAU), P.O. Box 1982, Dammam, 31441, Saudi Arabia

ARTICLE INFO

Article history:
Received 10 November 2022
Received in revised form
9 January 2023
Accepted 8 February 2023
Available online 14 February 2023

Keywords:
Zircon mineral
NASICON compounds
Calcination temperature
Radiation shielding properties
Monte Carlo simulation

ABSTRACT

The present work aims to fabricate $Na_{1+x}Zr_2Si_xP_{3-x}O_{12}$ compound at various calcination temperatures based on the zircon mineral. The fabricated compound was calcinated at 250, 500, and 1000°C. The effect of calcination temperature on the structure, crystal phase, and radiation shielding properties was studied for the fabricated compound. The X-ray diffraction diffractometer demonstrates that, the monoclinic crystal phase appeared at a calcination temperature of 250°C and 500°C is totally transformed to a high-symmetry hexagonal crystal phase under a calcination temperature of 1000°C. The radiation shielding capacity was also qualified for the fabricated compounds using the Monte Carlo N-Particle transport code in the γ-photons energy interval between 15keV and 122keV. The impacts of calcination temperature on the γ-ray shielding behavior were clarified in the present study, where the linear attenuation coefficient was enhanced by 218% at energy of 122keV, when the calcination temperature increased from 250 to 1000°C, respectively.

1. Introduction

More than half a century ago, the NASICON (sodium ion fast conductivity) model showed in its formula ($Na_{1+x}Zr_2Si_xP_{3-x}O_{12}$) an electrolyte in the solid state superconducting sodium ions. The phase behavior of this conductor in which (0<X > 3) is formed by increasing temperature [1]. The NASICON model is usually manufactured by calcination at higher temperatures greater than 1200 °C. As a result of the high temperature, phases of monoclinic zirconia impurities ZrO_2 and monoclinic silica SiO_2 have appeared due to the changing conditions of sodium and phosphorous [2]. The emergence of SiO_2 and ZrO_2 as impurities in this highly conductive form loses the NASICON advantages as well as reduces the conducting capacity due to the transformation of the crystalline phase to another form [3]. In order to overcome these impurities, Von Alpen and many researchers presented studies to decrease ZrO_2 from the NASICON model, but sometimes they presented phases that were not stable in aqueous solutions [4]. Several previous studies describe the fabrication of the NASICON model by using hydrothermal methods using zirconium phosphate [5]. The NASICON model structure ($Na_{1+x}Zr_2Si_xP_{3-x}O_{12}$) provides a versatile framework, incorporating both cationic (Na^+ and Zr^{4+}) and anionic (SiO_4^{-4} and PO_4^{-3}) moieties which enable the number of Na^+ ions to vary between 1 and 4 per formula unit with the corresponding changes in the P/Si ratio and Na^+ ion conductivity [6]. NASICON models framework ($Na_{1+x}Zr_2Si_xP_{3-x}O_{12}$) exists in different phases formed at different temperatures that cause changes in the lattice parameters [7].

On the other hand, gamma rays are high-energy electromagnetic radiation that can cause damage to live tissues and cells. For

* Corresponding author. Nuclear Materials Authority, P.O. Box 530 El-Maadi, Cairo, Egypt.
** Corresponding author.
E-mail addresses: islam.alhindawy@gmail.com (I.G. Alhindawy), karemabdelazeem@yahoo.com (K.A. Mahmoud).

https://doi.org/10.1016/j.net.2023.02.014

this reason, an in-depth investigation is needed with the goal of determining whether or not the usage of gamma radiations is safe and appropriate. The production of gamma ray shielding is an interesting topic of interest that has increased greatly in recent years due to the release of radioactive materials, the rising need for radiotherapy, and the proliferation of nuclear weapons. The primary goal of radiation shielding is to safeguard living things from the potential dangers of gamma radiation. It is necessary to have a knowledge of the deep penetration capabilities of gamma photons in order to design shields that are efficient for the treatment of radioactive waste. In the literature, a lot of recent papers have studied the radiation shielding performance of different useful materials such as concretes, glasses, Ceramics, and polymers [8–14], while no one study the ability of the NASICON model to attenuate the electromagnetic radiation such as X-ray and γ-ray.

The novelty of the present study is to estimate the impacts of calcination temperature on the synthesis, structure, and the γ-ray shielding properties of a NASICON compound based on the Egyptian zircon mineral.

2. Experimental

2.1. Synthesis procedure

(i) Creation of Zirconium oxychloride ($ZrOCl_2 \cdot 8H_2O$) and sodium silicate (SiO_2: Na_2O) were obtained by combining zircon mineral ($ZrSiO_4$ compound has a purity of 97%) with sodium hydroxide (NaOH compound has a purity of 95.9%) in a 316-L stainless steel open crucible at 700°C for 3 h [15]. After that stirred the fusion product with dis. H_2O for 3h for washing then filtrating to separate the sodium silicate (Na_2SiO_3) which is soluble in water from insoluble sodium zirconate (Na_2ZrO_3). **(ii)** powder sodium silicate obtained by totally fuming of liquor and drying at 110 °C to obtain sodium silicate (SiO_2: Na_2O 1:3). **(iii)** The insoluble dried sodium zirconate treated with hydrochloric acid (HCl) (12 M) to generate zirconium oxychloride ($ZrOCl_2.xH_2O$), which was then cooled to form the crystalline structure. Decantation, filtration, and air drying were used to separate the framed crystals from the mother liquor, yielding a white powder of $ZrOCl_2.8H_2O$. **(iv)** A hydrothermal reaction was utalized to produce the sodium zirconium silico-phosphates ($Na_{1+x}Zr_2Si_xP_{3-x}O_{12}$) throught mixing 1 g of $ZrOCl_2 \cdot 8H_2O$ and 2 g of sodium silicate (SiO_2: Na_2O 1:3) with 0.7 mL of orthophosphoric acid H_3PO_4 (85 wt% solutions), 0.3 mL hydrogen fluoride HF, 0.55 g ammonium dihydrogen phosphate $NH_4H_2PO_4$, 0.6 g urea, 0.5 ml Tributyl phosphate $C_{12}H_{27}O_4P$ then 80 mL dis.H_2O was added and finally add 0.5 g Sodium lauryl sulfate (SLS) with continuous stirring for 1h, then all component transferred into a 100 mL capacity Teflon-lined stainless steel autoclave. The autoclave was heated in an oven and the reaction mixture was sealed and heated at 170 °C for 35h. After cooling naturally, the mixture was stirred in excess of dis. H_2O and ethanol for washing. The solids were collected and isolated by filtration and washing more than once to remove any pollution and contaminations. Finally, the solids of sodium zirconium silico-phosphates were dried on air and were dried at 80°C for 5h then calcinated at (1) 250, (2) 500, and (3) 1000°C for 6h to obtain sodium zirconium silico-phosphates. Fig. 1 can illustrate the method of preparation of sodium zirconium silico-phosphates from zircon minerals.

XRD patterns were acquired using a PANalytical X'Pert Pro diffractometer set to 45 kV and 40 mA at 25 °C with monochromatic CuKα radiation with a wavelength of 0.15406 nm to understand the crystallographic phase. In the scan range of 10°–90°, the diffractograms were recorded with a step size of 0.013. Moreover, Scherrer's equation (1) was utilized to calculate the crystal grain size of the fabricated compounds at various

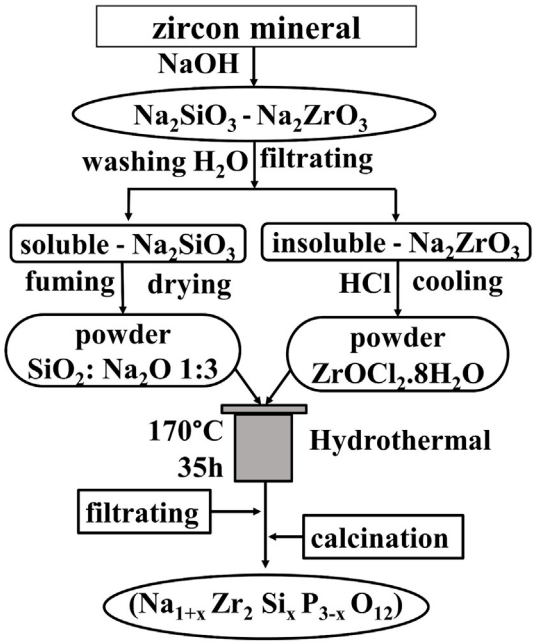

Fig. 1. Flow chart for the fabrication of NaSiCON compound from the Egyptian Rosetta zircon mineral.

temperatures [16].

$$L = \frac{K\,\lambda}{\beta\ COS\ \theta} \tag{1}$$

L, λ, β, and K refer to the nanocrystal size, XRD radiation wavelength (nm), the full width at the half maximum of peaks, and the shape factor takes values between 0.62 and 2.08.

2.2. γ-ray shielding capacity estimation

The Average track length (ATL) is simulated for the NASICON composites fabricated under various calcination temperatures using the MCNP code in the gamma photon energy (E_γ, keV) ranged 15 keV-122 keV [17]. The simulation of ATLs of the fabricated compounds required an input file containing all information and descriptions for the measuring system geometry. The aforementioned data was introduced to the input file via a variety of cards, including cell, surface, material, importance, source, tally, and physical cards. The cell is the main part of the input file where each component in the geometry was represented by a cell number and cell material. These rearranged cell dimensions and bounding surfaces were introduced to the input file's surface card. The importance card is that card controlled the photon passing through the arranged cells where the importance card is set to be 1 for cells in which the radiation pass while it is set to be zero for cells in which the radiation should be prevented to pass through. In addition, the material card is in charge of introducing the chemical composition of each cell in the input file. The source card, which should contain the position of the radioactive source, the cell number, the type of radiation emitted, the emitted photons distribution, and the photon direction, is one of the most important cards that should be correctly arranged. In the present study, a cylindrical source with a diameter of 1.5 cm and thickness of 0.5 cm was placed in the center of the arranged geometry at (0 0 0). The mentioned source emits photons with an energy range extending from 15 keV to 122 keV along Z directions. The tally used in the present study is F4. The mentioned F4 tally is used to evaluate the average flux per unit cell

of the fabricated compound cells. Then, the mentioned average flux per unit cell is used to estimate the average track length (ATL) of γ-photons inside the material cells. The cutoff card is considered one of the main and important physical cards, it is responsible for stopping the emission of photons to stop the interactions of photons with material electrons. The cutoff card can be expressed as a function of time (stopping the emission after a certain amount of time) or of historical number (stopping emission after a certain number of historical). The cutoff card was used in the current work in a second expression form, where it is defined to stop the emission after 10^6 historical. Finally, the input file is set to extract the interaction cross-section from the ENDF/B-VI.8 library data. After a successful running of the MCNP simulation, an output file was created. The mentioned output file contains the values of ATL for the prepared materials and also the statistical relative error in the simulation process which appears to be less than±1%. The simulated values for the ATL were utilized to evaluate the shielding properties such as the Linear attenuation coefficient (μ), Mass attenuation coefficient (μ_m), half-value thickness ($\Delta_{0.5}$), TF, and RPE, using the following equations (2)–(6) [18–21].

$$\mu\left(cm^{-1}\right) = \frac{1}{x}\ln\left(\frac{I_o}{I_t}\right) \tag{2}$$

$$\mu_m\left(\frac{cm^2}{g}\right) = \frac{\mu\left(cm^{-1}\right)}{\rho\left(\frac{g}{cm^3}\right)} \tag{3}$$

The $\Delta_{0.5}$ is proportional to the μ values in the following way.

$$\Delta_{0.5}\ (cm) = \frac{\ln(2)}{\mu} \tag{4}$$

The TF and the RPE are given in equations (5) and (6):

$$TF\ (\%) = \frac{I_t}{I_o} \times 100 \tag{5}$$

$$RPE\ (\%) = \frac{I_a}{I_o} \times 100 \tag{6}$$

3. Results and discussion

Fig. 2 shows the XRD profiles for the fabricated $Na_{1+x}Zr_2Si_xP_{3-x}O_{12}$ compounds at various temperatures in the 2θ interval between 10 and 90° [22]. The monoclinic phase existing at 250, 500 ^{O}C in NASICON gradually transforms to the high-symmetry hexagonal phase on raising the temperature to 1000 ^{O}C. It is worth noting that most of the XRD peaks in all phases lie very close to each other and therefore overlap. It was possible to distinguish between the different phases of the XRD pattern at the positions of the different peaks as shown in Fig. 3a, b, and c to show the phases of compounds formed at each temperature. At temperatures of 250 and 500 °C, the NASICON form is in the monoclinic phase with a ratio of 28 and 23% with chemical composition ($P_{4.36}O_{48}Na_{8.96}Zr_{7.52}Si_{7.64}$) and ($O_{48}P_4Si_8Na_{12}Zr_{7.72}$), respectively [23,24]. The compound ($Na_8Zr_4Si_{12}O_{44}$) is also in the Orthorhombic phase with a percentage of 36% and 39%, respectively [25]. Silica oxide ($Si_{16}O_{32}$) was also present in proportions of 37% and 21%, respectively [26,27]. As a result of the increase in calcination on the main axes with an increase in temperature to 1000 °C, the angles between the axes changed, which led to the formation of the hexagonal phase in the crystals, thus forming NASICON compounds ($P_{17.33}Na_{6.86}O_{72}Zr_{12}Si_{0.67}$, $P_{4.5}O_{72}Na_{19.32}Si_{13.5}Zr_{12}$) [1,28] by up to

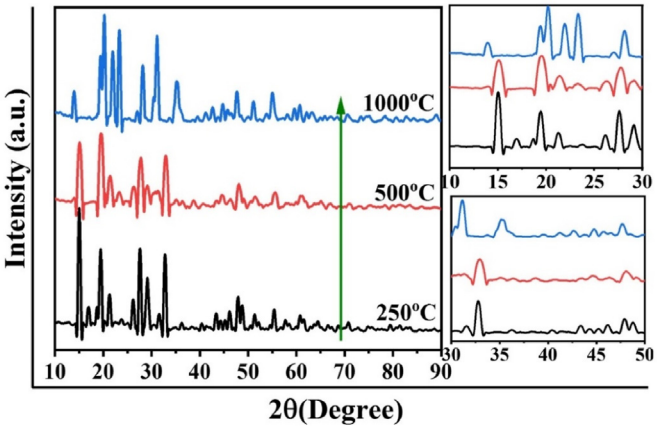

Fig. 2. X-ray diffraction (XRD) of the collected sample at different temperatures.

80% with the presence of some impurities of hexagonal $Si_2P_4O_{18}$ by 20% [29]. Fig. 3d shows the geometric diagram of the shape of a NASICON crystal in three different phases and Table 1 can also show the crystal parameters. The average crystal size of the collected nanomaterials at 250, 500, and 1000 °C was 16.86, 15.24, and 14.91 nm, respectively, as calculated by Scherrer's equation (Fig. 4). The decrease in crystal size of the samples further confirms disappearance of impurities and the formation of the NASICON compound.

The Monte Carlo N-Particle transport simulation code was applied to evaluate the average track length (ATL) of incident γ-photon inside the fabricated NASICON compound in the γ-photon energy (E_γ) between 15 and 121keV. Fig. 5 illustrates the influence of raising the incident E_γ on the μ_m of the fabricated compounds. The computer simulation data shows that raising the incident E_γ followed by a strong μ_m reduction for the NASICON composite under various temperatures (250°C, 500°C, and 1000°C). For example, the newly synthesised composites' μ_m values decline between 7.80-0.18cm^2/g (under a temperature of 250 °C), 7.88-0.18cm^2/g (under a temperature of 500°C), and between11.94-0.31cm^2/g (under a temperature of 1000°C). The early mentioned high decrease in the μ_m values has been assigned to the photoelectric (PE) interaction with a cross-section reversely varied to the $E^{3.5}$. Fig. 5 depicts a strong peak between 15 and 20 keV, which appears for sample 1000°C only. This peak is attributed to the K-absorption edge of Zr which is concentrated in the sample fabricated under 1000°C. Moreover, the mentioned figure depicts an agreement between simulated μ_m values and the calculated theoretically using the XCOM software for the fabricated NASICON composites.

The influence of the fabrication temperature on the μ_m of NASICON compounds is illustrated in Fig. 6. The simulated data depicts that μ_m values of the fabricated composites raised as the excess of fabrication temperature. At E_γ of 15 keV, the NASICON compounds' values enhanced by 53 % (from 7.8 cm^2/g to 11.94 cm^2/g), enriching the calcination temperature between 250 ^{O}C and 1000 ^{O}C, respectively. The same increasing trend in the NASICON compounds' μ_m values was observed at all studied energies likewise 59keV, and 121keV for example. The previous increase in the μ_m values is due to the PE interaction where the PE cross section is in proportion with the effective atomic number (Z_{eff}^{4-5}). In the present study, raising the fabrication temperature causes a significant variation in the crystal phase of the NASICON compound where at 250°C the crystal phases are Monoclinic and Orthorhombic with chemical formulas of $P_{4.36}O_{48}Na_{8.96}Zr_{7.52}Si_{7.64}$, $Na_8Zr_4Si_{12}O_{44}$ and

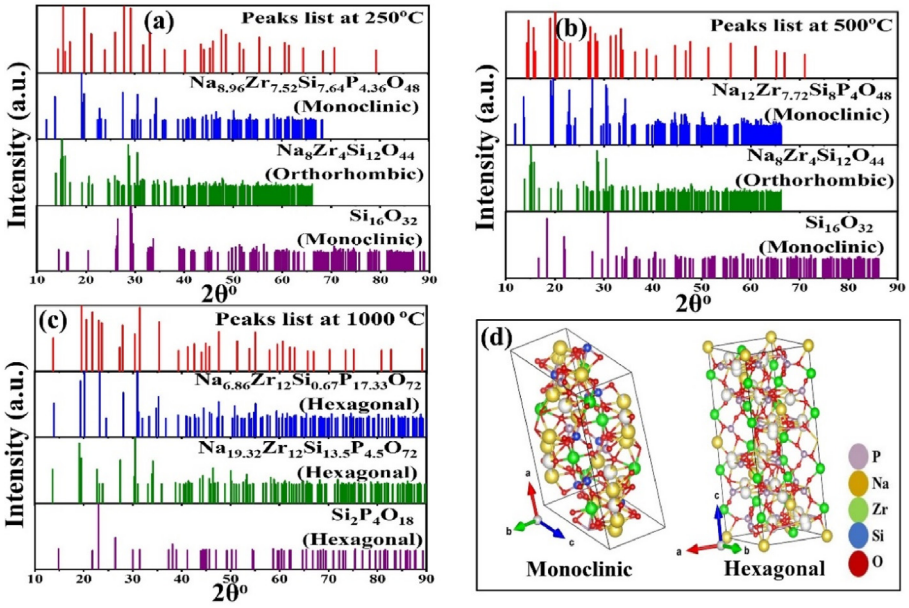

Fig. 3. The different phases of the XRD pattern at the positions of the different peaks at different temperatures (a) 205°C, (b) 500°C, (C) 1000°C, and (d) the shape of the NASICON crystal phase.

Table 1
The crystal lattice parameters for NASICON compounds at different temperatures.

Temperature (°C)		250	500	1000
Phase		Monoclinic	Monoclinic	Hexagonal
Lattice type		C	C	R
Space group		C 2/c	C 2/c	R −3 c
Lattice parameters	a	15.6451	15.6428	8.809
	b	9.0491	9.0484	8.809
	c	9.2151	9.2214	22.929
	alpha	90	90	90
	beta	123.724	123.871	90
	gamma	90	90	120

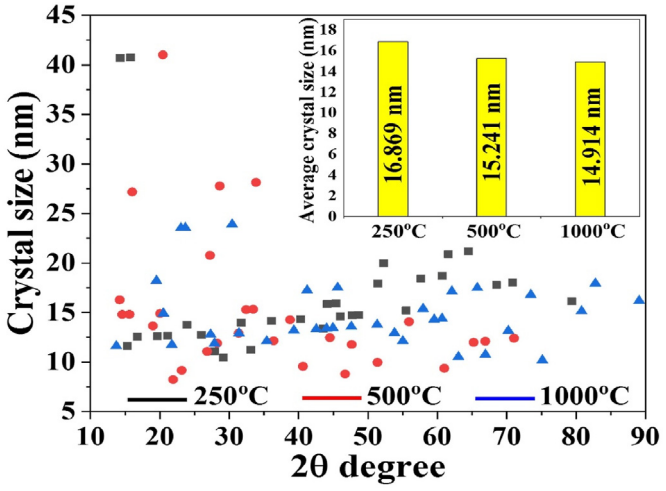

Fig. 4. The crystal size of collected samples at different temperatures using Scherrer's equation and inset figure is the average crystal size.

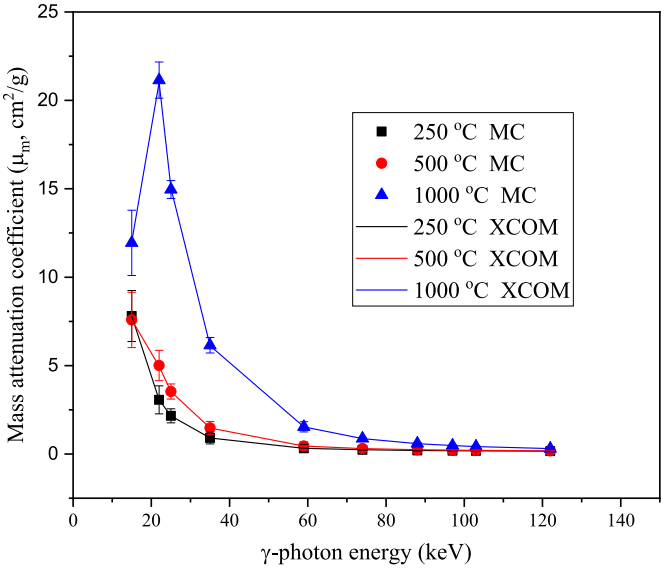

Fig. 5. Variation of the mass attenuation coefficient against the E_γ values for the fabricated NASICON compound under various temperatures (250, 500, 1000 °C).

some impurities of Monoclinic ($Si_{16}O_{32}$). A 500°C the XRD characterization showed that the NASICON compound has the same crystal phase of Monoclinic and Orthorhombic but different in the chemical composition $O_{48}P_4Si_8Na_{12}Zr_{7.72}$, $Na_8Zr_4Si_{12}O_{44}$, and also

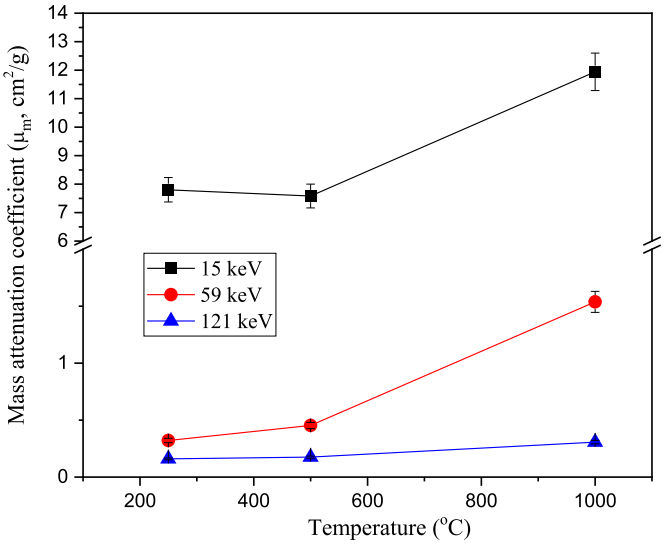

Fig. 6. Effect of temperature on the mass attenuation coefficient (μ_m, cm^2/g), at various E_γ energies.

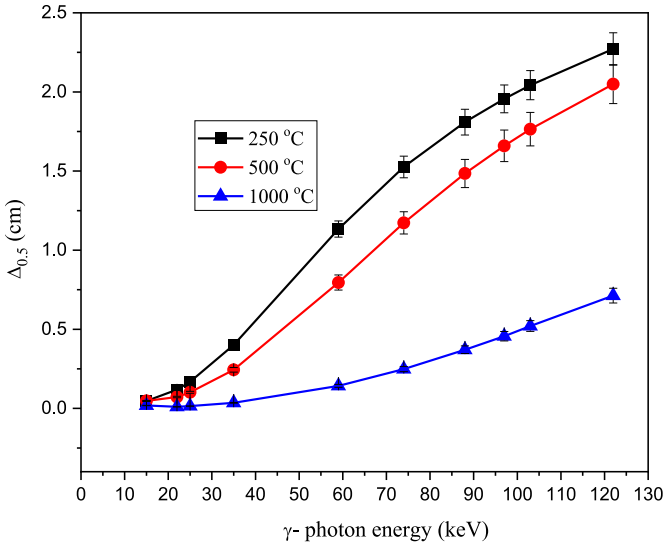

Fig. 7. Variation of the half-value thickness against the γ-photon energy (E_γ).

the presence of the Monoclinic ($O_{32}Si_{16}$). Finally, at a temperature of 1000°C, all crystal phases in the compound transferred to Hexagonal with a chemical formula of $P_{17.33}Na_{6.86}O_{72}Zr_{12}Si_{0.67}$, $P_{4.5}O_{72}Na_{19.32}Si_{13.5}Zr_{12}$, and $Si_2P_4O_{18}$. According to the previous discussion, it is clear that the Zr was concentrated in the samples fabricated under a temperature of 1000°C, and its concentration decreased with decreasing the fabrication temperatures to 500 and 250°C. As a result, the Z_{eff} of the sample fabricated under the temperature of 1000°C is the highest followed by the samples fabricated under 500°C and 250°C. Thus, the capacity of the sample 1000°C is high compared to the other fabricated sample at temperatures 500°C and 250°C.

Fig. 7 illustrates the influence of the E_γ on the $\Delta_{0.5}$ for the fabricated NASICON composite under various temperatures of 250, 500, and 1000°C. For all fabricated composites, the $\Delta_{0.5}$ values have an increasing trend with an increase in the emitted E_γ values. The calculated $\Delta_{0.5}$ values grow between 0.047cm and 2.27cm (for a sample fabricated under a temperature of 250°C), increases from 0.048cm to 2.049cm (for a sample fabricated under a temperature of 500°C), and from 0.018cm to 0.713cm (for sample fabricated under a temperature of 1000°C) with increasing the E_γ values between 15 and 121keV. Due to the γ-photons' high penetration power, which rises as the E_γ value is raised, the calculated $\Delta_{0.5}$ values have increased significantly. Thus, the incoming photons easily penetrate the fabricated composite material. As a result, the μ of the fabricated NASICON composite diminished associated with an increase in the required $\Delta_{0.5}$ values, where $\Delta_{0.5} = 0.693/\mu$.

The composites' fabrication temperatures were observed to have a strong effect on the $\Delta_{0.5}$ and relation length (λ, cm) values, where the relation length is the average distance between two followed collisions between the γ-photons and the composites atoms. Fig. 8 refers that both $\Delta_{0.5}$ and λ values have a reduction trend with raising the composites fabrication temperature. For example, the calculated $\Delta_{0.5}$ values were reduced by 87.4% (from 1.134cm to 0.142cm) by raising the composite fabrication temperatures from 250 to 1000°C, respectively. The λ values have the same trend as the $\Delta_{0.5}$ values but it decreases between1.636cm-0.205cm with raising the composites fabrication temperatures. The mentioned decreasing trend is related to the transfer that occurred in the crystal phase with raising the fabrication temperature where the crystal phases Monoclinic, Orthorhombic, and Monoclinic in the fabricated composites under fabrication temperatures of 250 and 500°C transferred to Hexagonal in the composite fabricated under 1000°C. This transfer is associated with a significant increase in the Zr concentration in the fabricated composites, especially at 1000°C. This increase in the Zr concentration in the fabricated samples under a temperature of 1000°C resists the passing of γ-photons. As a result, the simulated μ values for fabricated NASICON composites increases followed by a reduction in the $\Delta_{0.5}$ and λ values where $\Delta_{0.5} = 0.693/\mu$ and $\lambda = 1/\mu$.

The TF denotes the ratio of photons penetrate the composite thickness to the net photons emitted by the utilized radioactive source. The TF values are totally opposite to the RPE, as illustrated in Fig. 9. The TF values increased from 0% to 37.8% while the RPE reduced from 100% to 62.18% associated with an increase in the E_γ from 15 to 121 keV, respectively, for 1 cm of the fabricated composite under a temperature of 1000 °C. Also, other samples fabricated under temperatures of 250°C and 500°C have the same trend of variation for the TF and RPE with the incoming E_γ. The higher the γ-photons energy, the higher the penetration power gained by photons. Thus, the photons move inside the fabricated composite freely with a low number of collisions between the emitted γ-

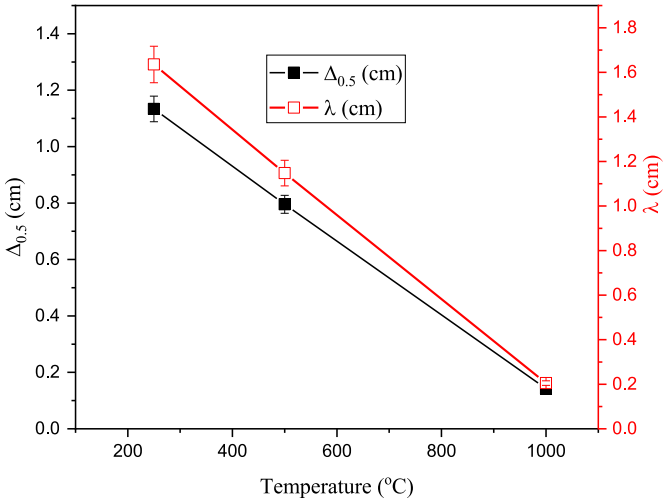

Fig. 8. Influence of the fabrication temperature on the NASICON's composites $\Delta_{0.5}$ and relaxation length (λ, cm) at E_γ of 59 keV.

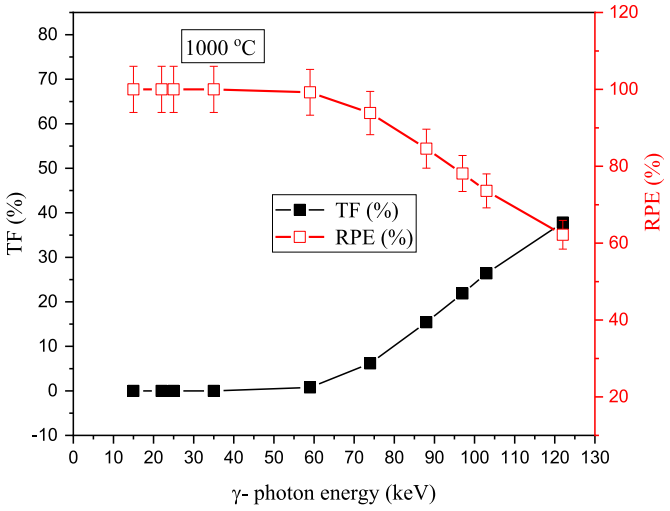

Fig. 9. The transmission factor and radiation protection efficiency for the current composite under temperature 1000 °C.

photons and the composite atoms which leads to an increase in the number of photons that escape from the composite thickness. The net result is an increase in TF values followed by an equivalent reduction in RPE values.

Growing the composite thickness causes, a notable improvement in the RPE and an equivalent reduction in the TF values, as shown in Fig. 10. Increasing the composite thickness greater than λ values, increases the γ-ray path length as well as the interaction probability between photons and the composite atoms and electrons. Thus, the amount of γ-energy consumed inside the composite thickness increases associated with an increase in the number of absorbed photons inside the composite thickness and a decrease in the number of photons penetrating the composite thickness. Therefore, the RPE increases accompanied by an increase in the TF values. At $E_\gamma = 59$keV, the composite fabricated under the temperature of 1000°C has RPE values exceeds from 38.6% to 99.2% while the TF values reduced from 61.45% to 0.77% linked with growing the NASICON composites' thickness between 0.1cm and 1cm, respectively.

Fig. 11 shows the influence of the fabrication temperature on the calculated values of TF and RPE at E_γ of 59keV. The TF values were

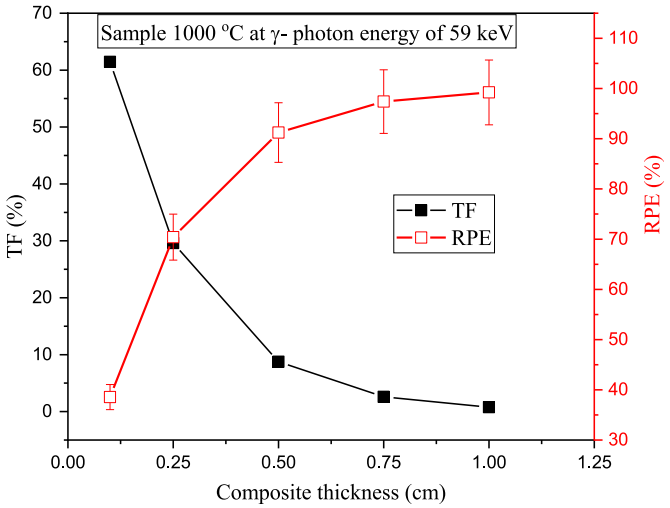

Fig. 10. The impacts of the composite thickness in TF and RPE values for the composite fabricated under the temperature of 1000 °C and at $E_\gamma = 59$ keV.

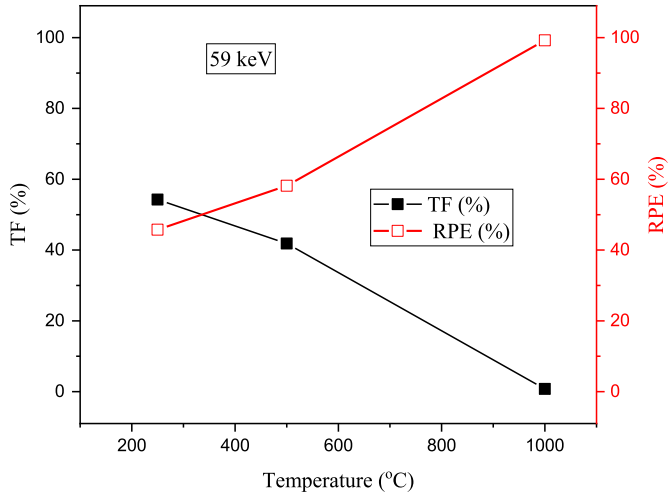

Fig. 11. Impacts of the fabricated composite temperature on the TF and RPE at E_γ of 59 keV.

reduced by 98% from 54.2% to 0.77% while the RPE increase with an equivalent value from 45.7% to 99.2% by raising the fabrication temperature from 250 to 1000 °C, respectively. These behaviors are related to the increase in Zr concentrations as well as the NASICON composites' Z_{eff} by raising the fabrication temperature. Therefore, the μ values increased followed by an increase in the I_a photons and a decrease in the I_t photons which leads to an increase in the RPE and an equivalent decrease in the TF values.

The previously mentioned data showed that the NASICON composites especially that fabricated under the fabrication temperature of 1000°C exhibited good γ-ray shielding capacity besides its high performance in the lithium ions battery.

4. Conclusions

The NASICON compounds which has high superconductivity properties was fabricated via hydrothermal reaction under various calcination temperatures based on zircon mineral. The influence of the calcination temperature on the structural characteristics as well as the gamma-ray shielding properties was studied. The XRD analysis depicts that the monoclinic phase existing in the NASICON compound at 250°C and 500°C was gradually transformed to a high-symmetry hexagonal phase under a fabrication temperature of 1000°C. Moreover, the Monte Carlo N-Particle simulation code clarifies that the radiation shielding properties of the fabricated compound are gradually enhanced by raising the calcination temperature. The study can conclude that the raising temperature between 250 and 1000°C causes a transformation in the crystal phase from monoclinic to symmetry hexagonal phase which causes an increase in the linear attenuation coefficient of the fabricated NASICON compounds. At 59keV, the μ values enhanced from $0.611cm^{-1}$–$4.869cm^{-1}$, with raising the fabrication temperature between 250 and 1000°C, respectively. The mentioned enhancement on the μ values of the fabricated compounds has a great effect on decreasing the $\Delta_{0.5}$ values where $\Delta_{0.5}$ values decreased by a factor of 87% with raising the fabrication temperature. The study can conclude that the NASICON compounds have good shielding properties against low energy gamma rays besides their good properties as a superconductivity material.

Declaration of competing interest

The authors declare that they have no known competing

financial interests or personal relationships that could have appeared to influence the work reported in this paper.

Acknowledgment

The authors express their gratitude to Princess Nourah bint Abdulrahman University Researchers Supporting Project number (PNURSP2023R2), Princess Nourah bint Abdulrahman University, Riyadh, Saudi Arabia.

References

[1] J.-P. Boilot, G. Collin, P. Colomban, Relation structure-fast ion conduction in the NASICON solid solution, J. Solid State Chem. 73 (1) (1988) 160–171.
[2] Francisco del Monte, Willa Larsen, John D. Mackenzie, Stabilization of tetragonal ZrO_2 in ZrO_2–SiO_2 binary oxides, J. Am. Ceram. Soc. 83 (3) (2000) 628–634.
[3] U. Von Alpen, M.F. Bell, H.H. Höfer, Compositional dependence of the electrochemical and structural parameters in the Nasicon system (Na1+x-SixZr2P3−xO12), Solid State Ionics 3–4 (1981) 215–218.
[4] U. von Alpen, M.F. Bell, W. Wichelhaus, Phase transition in nasicon (Na3Zr2-Si2PO12), Mater. Res. Bull. 14 (10) (1979) 1317–1322.
[5] R. Essehli, B. El Bali, S. Benmokhtar, K. Fejfarová, M. Dusek, Hydrothermal synthesis, structural and physico-chemical characterizations of two Nasicon phosphates: M0. 50IITi2 (PO4) 3 (M= Mn, Co), Mater. Res. Bull. 44 (7) (2009) 1502–1510.
[6] A. Clearfield, M. Subramanian, W. Wang, P. Jerus, The use of hydrothermal procedures to synthesize NASICON and some comments on the stoichiometry of NASICON phases, Solid State Ionics 9 (1983) 895–902.
[7] J.P. Boilot, G. Collin, R. Comès, Phase transition in Nasicon compounds Na3Sc2P3O12 and Na1+xZr2 (P3−xSix) O12, Solid State Ionics 5 (1981) 307–309.
[8] M.A. Khalaf, C.C. Ban, M. Ramli, The constituents, properties and application of heavyweight concrete: a review, Construct. Build. Mater. 215 (2019) 73–89.
[9] M.K.A. Roslan, M. Ismail, A.B.H. Kueh, M.R.M. Zin, High-density concrete: exploring Ferro boron effects in neutron and gamma radiation shielding, Construct. Build. Mater. 215 (2019) 718–725.
[10] Y. Ding, Z. Li, Z. Bai, Z. Jiang, Z. Chen, X. Zhang, C. Lu, H. Dan, T. Duan, Rapid preparation of Nd-doped zirconia ceramics for high-level radioactive waste immobilization, Ceram. Int. 48 (12) (2022) 16773–16777.
[11] M. Sayyed, E. Hannachi, K. Mahmoud, Y. Slimani, Synthesis of different (RE) BaCuO ceramics, study their structural properties, and tracking their radiation protection efficiency using Monte Carlo simulation, Mater. Chem. Phys. 276 (2022), 125412.
[12] M. Koubisy, K.S. Shaaban, E.A. Wahab, M. Sayyed, K. Mahmoud, Synthesis, structure, mechanical and radiation shielding features of 50SiO2–(48+ X) Na2B4O7–(2− X) MnO2 glasses, Eur. Phys. J. Plus 136 (2) (2021) 156.
[13] M. Almurayshid, S. Alsagabi, Y. Alssalim, Z. Alotaibi, R. Almsalam, Feasibility of polymer-based composite materials as radiation shield, Radiat. Phys. Chem. 183 (2021), 109425.
[14] C.V. More, Z. Alsayed, M. Badawi, A. Thabet, P.P. Pawar, Polymeric composite materials for radiation shielding: a review, Environ. Chem. Lett. 19 (3) (2021) 2057–2090.
[15] I.G. Alhindawy, E.A. Elshehy, M.E. El-Khouly, Y.K. Abdel-Monem, M.S. Atrees, Fabrication of mesoporous NaZrP cation-exchanger for U(VI) ions separation from uranyl leach liquors, Colloids Interf. 3 (4) (2019) 61.
[16] I.G. Alhindawy, H.I. Mira, A.O. Youssef, S.M. Abdelwahab, A.A. Zaher, W.A. El-Said, E.A. Elshehy, A.M. Abdelkader, Cobalt doped titania-carbon nanosheets with induced oxygen vacancies for photocatalytic degradation of uranium complexes in radioactive wastes, Nanoscale Adv. 4 (24) (2022) 5330–5342.
[17] X-5 Monte Carlo Team, MCNP — A General Monte Carlo N-Particle Transport Code, Version 5, La-Ur-03-1987. II, 2003.
[18] M. Sayyed, M.H.M. Zaid, N. Effendy, K.A. Matori, E. Lacomme, K. Mahmoud, M.M. AlShammari, The influence of PbO and Bi2O3 on the radiation shielding and elastic features for different glasses, J. Mater. Res. Technol. 9 (4) (2020) 8429–8438.
[19] A. Abouhaswa, M. Sayyed, A.S. Altowyan, Y. Al-Hadeethi, K. Mahmoud, Synthesis, structural, optical and radiation shielding features of tungsten trioxides doped borate glasses using Monte Carlo simulation and phy-X program, J. Non-Cryst. Solids 543 (2020), 120134.
[20] M. Sayyed, K. Mahmoud, S. Islam, O. Tashlykov, E. Lacomme, K.M. Kaky, Application of the MCNP 5 code to simulate the shielding features of concrete samples with different aggregates, Radiat. Phys. Chem. 174 (2020), 108925.
[21] K. Naseer, K. Marimuthu, K. Mahmoud, M. Sayyed, The concentration impact of Yb3+ on the bismuth boro-phosphate glasses: physical, structural, optical, elastic, and radiation-shielding properties, Radiat. Phys. Chem. 188 (2021), 109617.
[22] J.A.S. Oh, L. He, A. Plewa, M. Morita, Y. Zhao, T. Sakamoto, X. Song, W. Zhai, K. Zeng, L. Lu, Composite NASICON (Na3Zr2Si2PO12) solid-state electrolyte with enhanced Na+ ionic conductivity: effect of liquid phase sintering, ACS Appl. Mater. Interfaces 11 (43) (2019) 40125–40133.
[23] P. Rudolf, A. Clearfield, J. Jorgensen, A time of flight neutron powder rietveld refinement study at elevated temperature on a monoclinic near-stoichiometric NASICON, J. Solid State Chem. 72 (1) (1988) 100–112.
[24] P. Rudolf, A. Clearfield, J. Jorgensen, Rietveld refinement results on three nonstoichiometric monoclinic NASICONs, Solid State Ionics 21 (3) (1986) 213–224.
[25] G.Y. Chao, The crystal structure of gaidonnayite, Na 2 ZrSi 3 O 9. 2H 2 O, Can. Mineral. 23 (1) (1985) 11–15.
[26] L. Levien, C.T. Prewitt, High-pressure crystal structure and compressibility of coesite, Am. Mineral. 66 (3–4) (1981) 324–333.
[27] M.D. Foster, O. Delgado Friedrichs, R.G. Bell, F.A. Almeida Paz, J. Klinowski, Chemical evaluation of hypothetical uninodal zeolites, J. Am. Chem. Soc. 126 (31) (2004) 9769–9775.
[28] R. Hazen, L. Finger, D. Agrawal, H. McKinstry, A.J. Perrotta, High-temperature crystal chemistry of sodium zirconium phosphate (NZP), J. Mater. Res. 2 (3) (1987) 329–337.
[29] D. Poojary, R. Borade, F. Campbell III, A. Clearfield, Crystal structure of silicon pyrophosphate (form I) from powder diffraction data, J. Solid State Chem. 112 (1) (1994) 106–112.